



Effect of equal-channel angular pressing and aging on corrosion behavior of ZK60 Mg alloy

Xin LI¹, Jing-hua JIANG², Yong-hao ZHAO¹, Ai-bin MA², Dao-jing WEN¹, Yun-tian ZHU^{1,3}

1. School of Materials Science and Engineering, Nanjing University of Science and Technology, Nanjing 210094, China;

2. College of Mechanics and Materials, Hohai University, Nanjing 210098, China;

3. Department of Materials Science and Engineering, NC State University, Raleigh 27695, USA

Received 22 January 2015; accepted 2 July 2015

Abstract: Commercial ZK60 Mg alloy was processed by multi-pass equal-channel angular pressing (ECAP) and subsequent aging to investigate the effect of grain refinement and second-phase redistribution on its corrosion behavior. Electrochemical tests show that the fine-grained samples after more ECAP passes have higher corrosion current densities (J_{corr}) in the polarization curves, lower charge-transfer resistance (R_t) values in the EIS plots. The severe plastic deformation decreases the alloy corrosion resistance besides the well-known strengthening and toughening. Scanning Kelvin probe (SKP) measurement shows that the anodic and cathode sites are homogeneously distributed on the surface of the fine-grained alloy, which inhibits localized corrosion. The SKP potential, having linear relationship with the corrosion potential (φ_{corr}), decreases with increasing the ECAP pass. Furthermore, the post-ECAP aging can slightly improve the corrosion resistance of the fine-grained ZK60 Mg alloy and enhance the comprehensive performances, due to the stress relief and uniform distribution of second-phase particles.

Key words: ZK60 Mg alloy; equal-channel angular pressing; aging; corrosion resistance; fine-grains

1 Introduction

Mg and its alloys have been widely used in aerospace, portable microelectronics, telecommunication and military industry due to their low density, high specific strength and excellent recycle ability. However, the low standard electrode potential of Mg and the loose oxide film on the surface of Mg make its corrosion resistance poor in most environmental media, which hinders the application of Mg alloys. Therefore, the corrosion behaviors and corrosion protection of Mg alloys have received extensive attention in recent years.

The main factors affecting the corrosion resistance of metallic materials include the microstructure [1], second phases [2], chloride ion and pH value [3]. In view of excellent mechanical properties and promising applications of ultrafine-grained (UFG) alloys [4], the effect of grain refinement by various severe-plastic-deformation (SPD) methods on the corrosion behavior of metallic materials has caught considerable attention in

recent years. Equal-channel angular pressing (ECAP) is considered as the most appropriate SPD method to produce bulk UFG alloys for industrial application [5,6]. Although many studies have been done on the materials processed by ECAP [7,8], there are relatively few reports available on their corrosion resistance. Furthermore, the available literatures express contradictory views on the corrosion resistance of UFG alloys in comparison with their coarse-grained (CG) counterparts [9–13]. Grain refinement decreases the corrosion resistance of pure Mg [9], AZ31 Mg alloy [12] and AE21 Mg alloy [13] in corrosive media, but enhances the corrosion resistance of AE42 Mg alloy [13]. Now, UFG Mg alloys may have higher corrosion resistance than the coarse-grained ones, particular attention should be paid to the relationship between the microstructure change and corrosion behavior of the ECAP-processed Mg alloys.

Mg alloys are gradually used in structural applications and new classes of wrought Mg alloys are emerging. ZK60 Mg alloy, one of the representative wrought Mg alloys, has been successfully processed by

ECAP to markedly improve its mechanical properties [8,14]. However, appropriate corrosion resistance has not been achieved. The influence of microstructure parameters (such as the grain size, distribution of second phases, internal stress) on the corrosion behavior of UFG Mg alloys should be further investigated. The second-phase particles in ZK60 Mg alloy usually form the cathodes of electrochemical cells. The size and distribution of second-phase particles will be changed by ECAP and sequent heat treatment, which has great effect on the corrosion resistance of the UFG Mg alloys.

The objective of this study is to investigate the effect of microstructural evolution during processing by ECAP and post-ECAP aging on the corrosion behavior of ZK60 Mg alloy, which can provide guide for its application and perfect the corrosion theory study. Based on the previous researches [15,16], the post-ECAP aging of the alloy was done at 453 K to obtain better mechanical properties. Electrochemical tests were performed in a 3.5% NaCl (mass fraction) aqueous solution, complemented by morphological, structural and surface analysis. Scanning Kelvin probe (SKP) was used to investigate the atmospheric corrosion process on micro- and even nano-scale [17–20]. In the present work, the potentials of α -Mg matrix and second phases of the ZK60 Mg alloy with different ECAP passes and post-ECAP aging were studied by SKP to address the role of those fine second phases on the corrosion behavior, with the aim to better understand the influence of UFG microstructure on the corrosion behavior of ZK60 Mg alloy.

2 Experimental

2.1 Materials and ECAP process

Commercial ZK60 Mg alloy with a nominal composition of Mg–6Zn–0.5Zr (mass fraction, %) was used. The raw material used for the ECAP process was cut by an electric discharging machine from the as-cast ZK60 Mg ingots and then solid-solution (SS) treated at 703 K for 16 h. The billets after SS treatment were cut to the sizes of 20 mm × 20 mm × 40 mm and then equal-channel-angular-pressed at 518 K from 1 pass to 16 passes. To reduce the friction coefficient between the billet and the die inner wall, graphite was used as the lubricant. After each ECAP pass, the billet was inverted and then rotated by 180° on the same axes. After ECAP, all of the samples were cut perpendicularly to the pressing direction to the sizes of 10 mm × 10 mm × 8 mm. Then, the ECAP-fabricated samples were aged at 453 K for 8 h in a vacuum tube furnace under the protective gas of N₂.

2.2 Microstructure characterization

Optical microscopy (OM, ZEISS AXIO CSM700) was used to observe the microstructure of ECAP-processed ZK60 Mg alloy and the post-ECAP aged ones. Scanning electron microscopy (SEM, Oxford, USA) was used to observe the refined microstructure and the distribution of second phases in detail. All samples processed by ECAP and post-ECAP aging were, in turn, ground by 400, 600, 800, 1000, 1200 and 1600 grit emery papers and polished with diamond grinding fluid. The metallographic etchant consisted of 1 g oxalic acid, 1 mL nitric acid, 1 mL acetic acid and 150 mL deionized water.

2.3 Scanning Kelvin probe

The potential maps of the ECAP-processed ZK60 Mg alloy and the post-ECAP aged ones were recorded using SKP technique. The experiments were performed on VersaScan electrochemical scanning system (Princeton Applied Research, Ametek). Before testing, the samples were polished under the same conditions. All tests were carried out at the same ambient temperature and relative humidity. Step scan mode was employed, with a step size of 50 μm, a scan area of 1000 μm × 1000 μm, and scan points of 21 × 21. Each scan takes about 21 min.

2.4 Corrosion tests

The corrosion behavior of the ECAP-processed ZK60 Mg alloy and the post-ECAP aged ones were investigated by electrochemical test. All samples were cut from the core of the ECAP billets, cleaned and polished to avoid surface contamination of the lubricant. The corrosive agent used is 3.5% NaCl (mass fraction) solution prepared by A.R. grade NaCl and deionized water at room temperature.

Electrochemical tests were conducted in the 3.5% NaCl solution via VersaScan electrochemical scanning system, which employed a saturated calomel reference electrode, a Pt counter electrode and a working electrode as a traditional three-electrode system. The samples, cut from the core of the billets, were molded in the epoxy resin with an exposed surface of 1 cm². For good repeatability, all samples were polished, cleaned with acetone and dried in air.

Three types of electrochemical tests, namely open-circuit potential (OCP) test, potentiodynamic polarization test and electrochemical impedance spectroscopy (EIS) test, were carried out to compare the corrosion resistance of the ECAP-processed samples with the post-ECAP aged ones. All samples were immersed in the 3.5% NaCl solution for 1800 s to

achieve stable OCP values, and potentiodynamic polarization tests were performed at a scan rate of 2 mV/s. The frequency of EIS tests ranges from 100 kHz to 100 mHz, and the amplitude of sinusoidal potential signal is 5 mV with respect to the open circuit potential.

3 Results

3.1 Microstructure of ECAP-processed ZK60 Mg alloy

Figures 1(a) and (b) present the microstructures of the as-cast ZK60 Mg alloy and the solution-treated one, respectively. The grain size of the as-cast sample is 100–200 μm . After solution treatment, the branch-shaped grain boundaries almost disappear and the intergranular second phases are mostly dissolved into the Mg matrix. Only a few precipitates can be seen along the grain boundaries.

From Fig. 2, it can be seen that after the first ECAP pass (1p), some extremely fine grains are located on the

boundaries of large grains, suggesting that the deformation and grain refinement start firstly at the grain boundaries (GBs) of the ZK60 Mg alloy. In the 4-pass sample (4p), the deformed regions with UFG grains become thicker and the un-deformed grains are broken and become elongated with a finer grain size. In the 8-pass sample (8p), the fraction of deformed regions is predominant with some elongated un-deformed grains embedded inside the UFG region. The rest un-deformed grains are one order of magnitude smaller than those in the 4-pass sample. When the number of ECAP passes increases to 12 and 16, respectively, the un-deformed grains become even less. Hence, more ECAP passes lead to a sharp decrease of grain size.

After aging, the grain size of the α -Mg phase does not grow significantly, as seen in Fig. 3. The microstructure of the solution-treated sample changes to a flower shape, and the number of fine second phases of the ECAP-processed samples slightly increases, as shown in Figs. 3 and 4. The redistribution of second

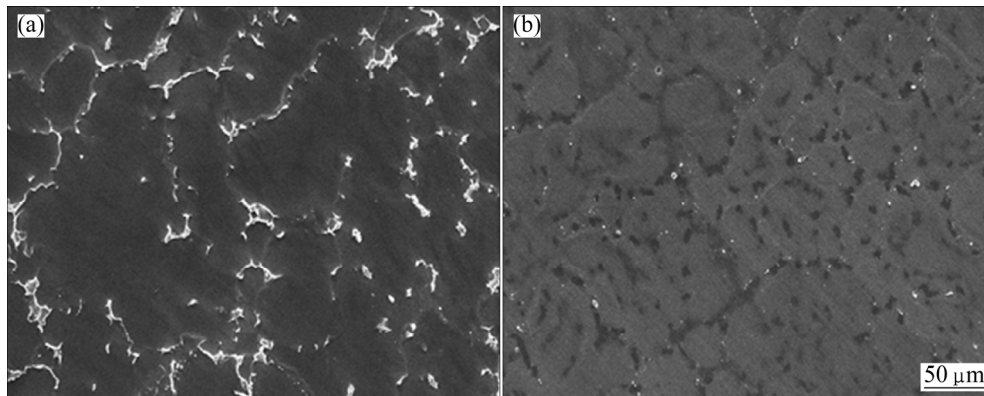


Fig. 1 SEM images of as-cast ZK60 Mg alloy (a) and solution-treated one at 703 K for 16 h (b)

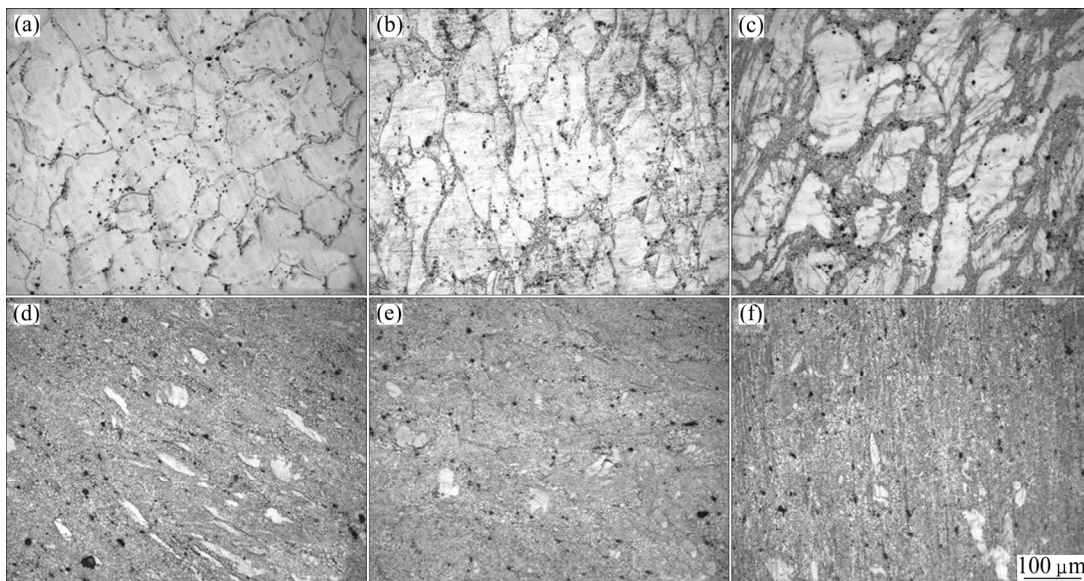


Fig. 2 Optical micrographs of solution-treated ZK60 Mg alloys with different ECAP passes: (a) Solution-treated sample; (b) 1p (1 ECAP pass); (c) 4p; (d) 8p; (e) 12p; (f) 16p

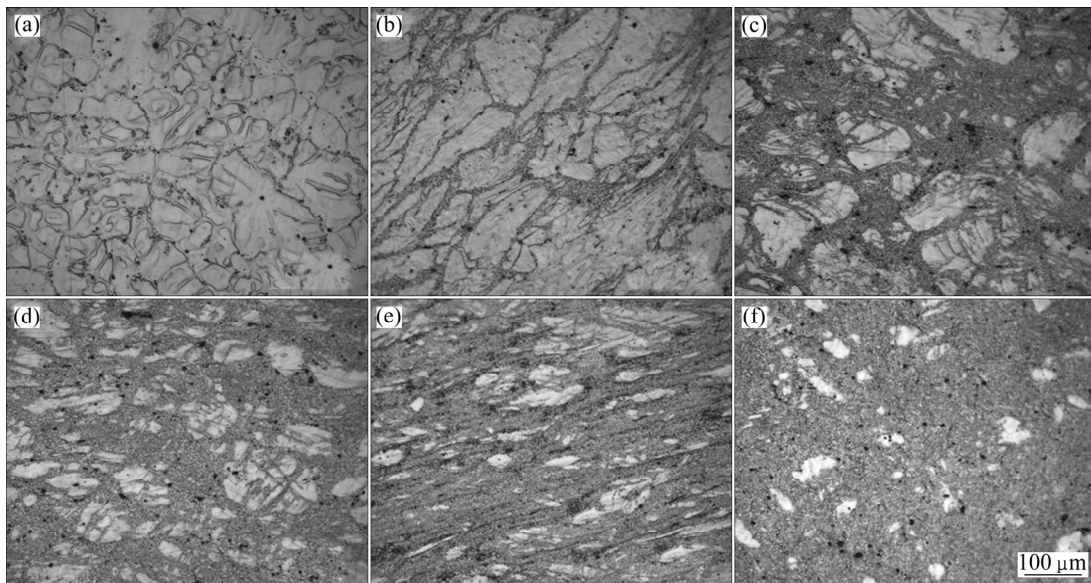


Fig. 3 Microstructures of solution-treated ZK60 Mg alloys after aging with different ECAP passes: (a) Solution-treated sample; (b) 1p (1 ECAP pass); (c) 4p; (d) 8p; (e) 12p; (f) 16p

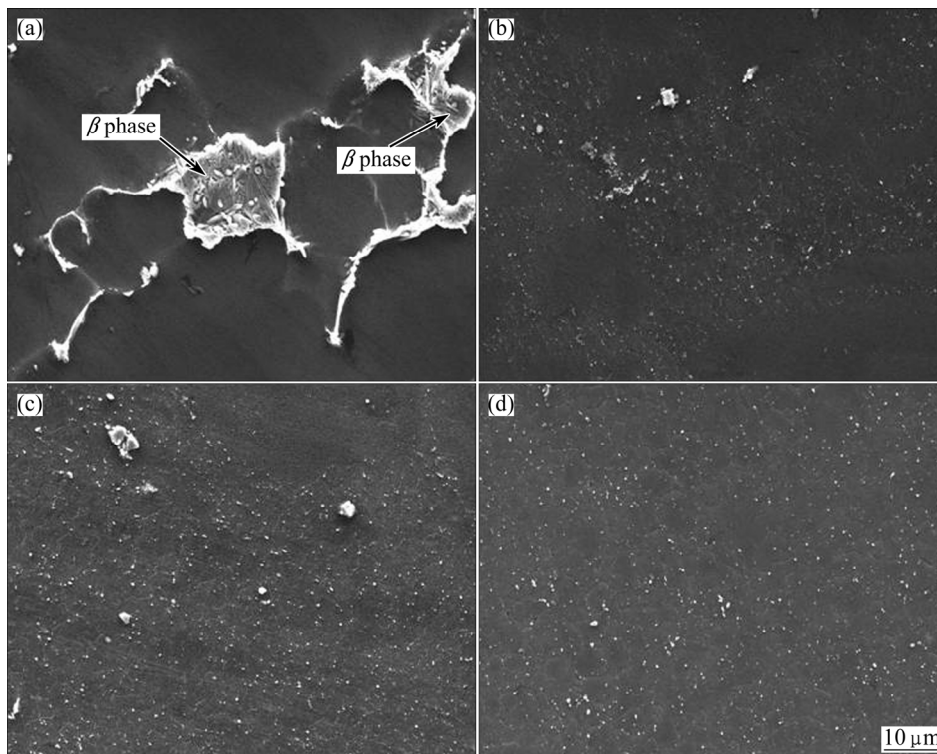


Fig. 4 SEM images of ZK60 Mg alloys in different processing states: (a) As-cast; (b) After 4 ECAP passes; (c) After 16 ECAP passes; (d) 16 ECAP passes plus post-aging

phase after aging can influence the corrosion behavior of the samples. As a result of SS treatment and ECAP, the coarse secondary phases along the grain boundaries in the as-cast alloy, as shown in Fig. 4(a), disappear and smaller particles are homogeneously distributed in the Mg matrix processed by ECAP, as shown in Fig. 4(c).

3.2 Electrochemical corrosion behavior

Electrochemical tests were performed to obtain the

electrochemical data of the ZK60 Mg alloy processed by ECAP. Figure 5 shows the OCP curves of the ECAP-processed samples and the post-ECAP aged ones immersed in 3.5% NaCl solution for 1800 s, which reveals the variation of electrode potential with the immersion time. All of the curves have a similar shape, which implies their similar electrochemical behavior. The curves of the ECAP-processed samples can be divided into two stages, i.e., the OCP values of all the

samples increase quickly at first and then fall down slightly with little fluctuation. The 16p sample has the lowest OCP value and takes the least time to reach the peak value, which implies the faster formation of $Mg(OH)_2$ in 3.5% NaCl solution. The solution-treated sample has a higher OCP value and takes more time to reach the peak value. The OCP curves of the post-ECAP aged samples are similar to those of the ECAP-processed ones, which indicates their similar electrochemical behavior. However, OCP is the value of the working

electrode relative to the reference electrode in the absence of additional current or electric field, which can not reflect the corrosion behavior accurately. Thus, further electrochemical tests still need to judge the corrosion resistance of the ECAP-processed alloy and the post-ECAP aged alloy clearly.

The potentiodynamic polarization curves of the ECAP-processed ZK60 Mg alloys and the post-ECAP aged ones are shown in Fig. 6. All samples were immersed in 3.5% NaCl solution for about 30 min before

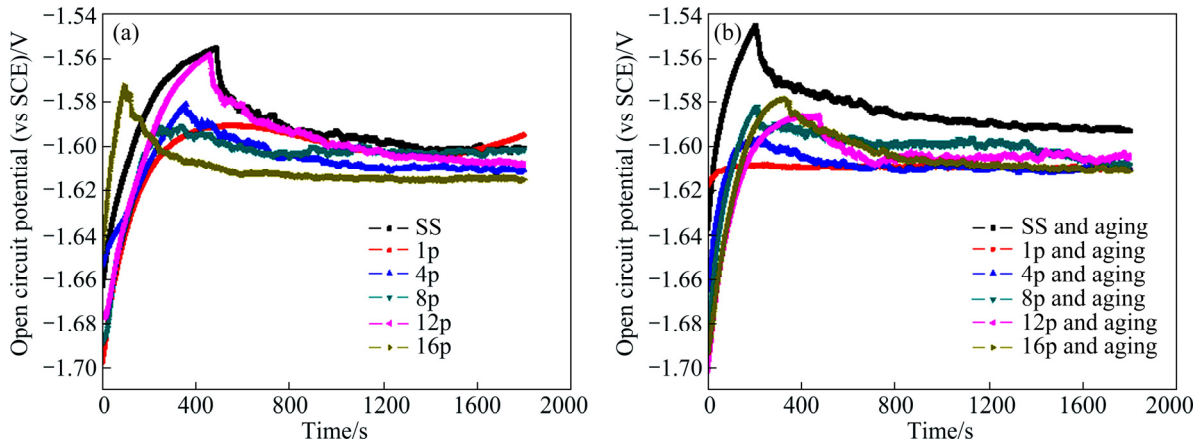


Fig. 5 Open circuit potential of ECAP-processed alloy (a) and aged alloy (b) immersed in 3.5% NaCl solution

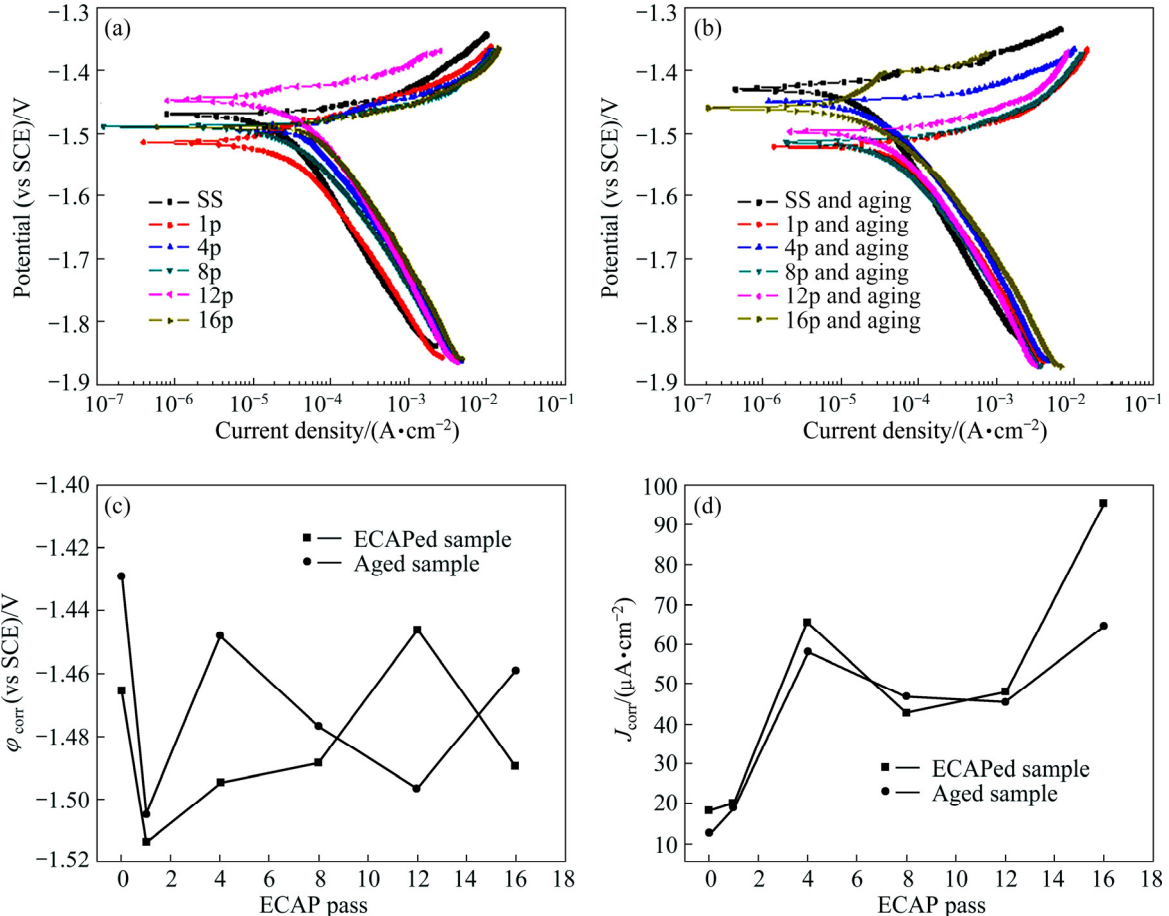


Fig. 6 Potentiodynamic polarization curves of ECAP-processed samples (a) and aged samples (b) immersed in 3.5% NaCl solution, ϕ_{corr} of ECAP-processed samples and aged samples (c) and J_{corr} of ECAP-processed samples and aged samples (d)

polarization tests to achieve stable OCP values, and the polarization curves of these samples are similar in the tested solution. The comparison of Figs. 6(a) with (b) shows that the curves of the solution-treated sample and the 16-pass one shift to the upper left side significantly, and the anode parts are more noble after post-ECAP aging. It implies lower corrosion current density (J_{corr}) and higher corrosion potential (φ_{corr}), i.e., better corrosion resistance. The φ_{corr} and J_{corr} values of the ECAP-processed ZK60 Mg alloys and the post-ECAP aged samples can be obtained from the polarization curves. The J_{corr} values were determined by extrapolating the linear Tafel segments of the anode and cathode polarization curves, which can be obtained from the testing software. From Fig. 6(c), it can be seen that the φ_{corr} values have no good regularity. In fact, the value of free corrosion potential does not represent the kinetics of material corrosion, but a thermodynamic characteristic of a given metal–electrolyte system [4]. Hence, the corrosion resistance can be usually judged from J_{corr} . Figure 6(d) presents that the 16p ZK60 Mg alloy has the highest J_{corr} , while the solution-treated sample has the lowest J_{corr} . It can be concluded that the corrosion resistance of Mg alloy basically decreases with increasing the ECAP pass, except the 4-pass sample. The exception can be ascribed to the higher dislocation density and deformation energy stored in grains. The J_{corr} values of post-ECAP aged samples are almost lower than those of only ECAP-processed ZK60 Mg alloy, especially the 16p and the solution-treated counterpart, which implies better corrosion resistance after the post-ECAP aging.

Figure 7 shows the SEM morphologies of the solution-treated sample and the 16p sample after being immersed in 3.5% NaCl solution for 4 h. It is found that the surface of the 16p sample after immersion is covered by thick and black corrosion products, while that of the solution-treated sample is only slightly corroded. The energy dispersive X-ray (EDX) results show that the main corrosion product is $\text{Mg}(\text{OH})_2$. It can be seen that the corrosion products have high porosity and micro-cracks (Fig. 7(b)). The cracks can be related to the high compressive stresses within the oxide layer [4], and the corrosion products provide nearly no protection against further corrosion. Figure 8 presents the surface morphologies of the solution-treated sample and the 16p sample after removing the corrosion products, there are some clear and shallow corrosion pits on the surface of the solution-treated sample, while the 16p sample surface is severely corroded with larger and deeper pits.

EIS tests were conducted to further investigate the electrochemical characteristics of the ECAP-processed alloy and the aged ZK60 Mg alloy. Figure 9 shows the Nyquist plots of the ECAP-processed samples and the

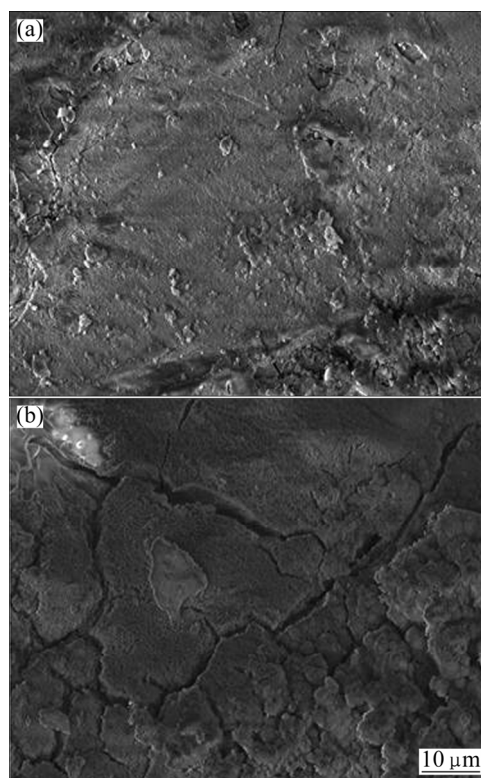


Fig. 7 Morphologies of solution-treated sample (a) and 16p sample (b) after immersion in 3.5% NaCl solution for 4 h

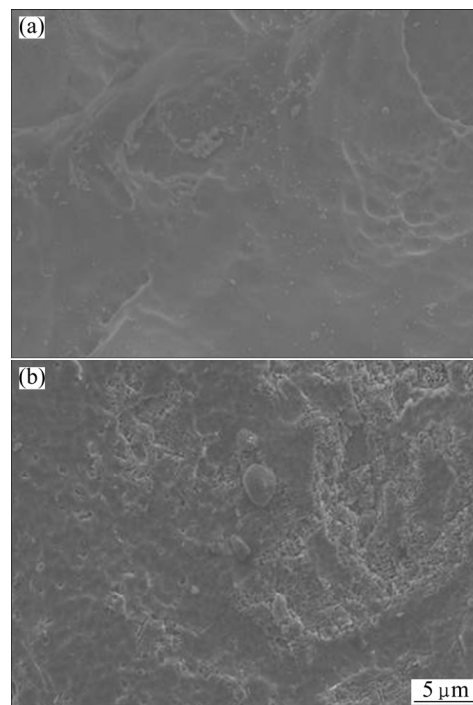


Fig. 8 Morphologies of solution-treated sample (a) and 6p sample (b) after removing corrosion product

aged samples after immersion in 3.5% NaCl solution at the initial 30 min. All plots reveal a capacitive arc at the high and intermediate frequencies. To better explain the corrosion behavior of the ZK60 Mg alloys, the arc in

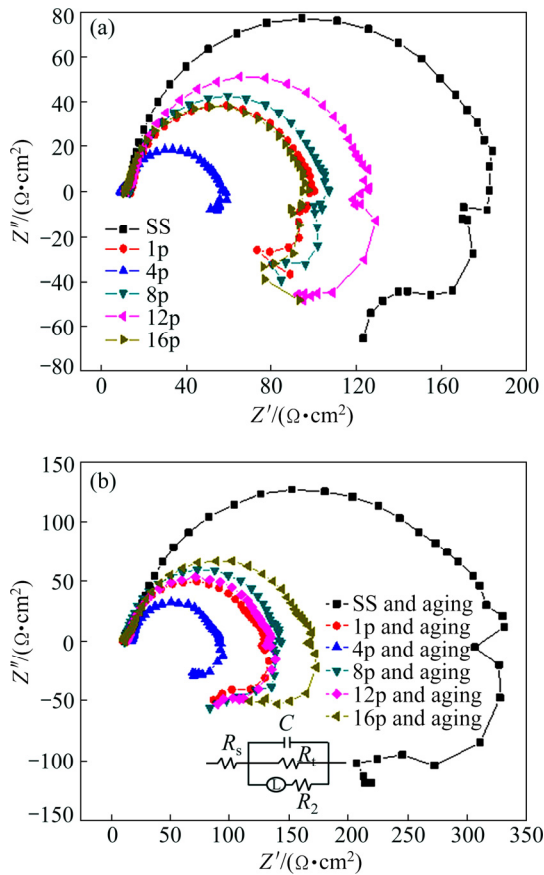


Fig. 9 Nyquist plot of ECAP-processed samples (a) and aged samples (b) immersed in 3.5% NaCl solution (Insert in Fig. 9(b) is equivalent circuit model)

the Nyquist plot is simulated by a Randles circuit with R_t (charge-transfer resistance), C (capacitance of double-layer or oxide film), R_s (electrolyte resistance), and R_2 (resistance of oxide film). An inductive element is incorporated into the simple Randle circuit, considering the inductive behavior observed at the low frequency. According to Refs. [21,22], this arc can be related to the metal dissolution in the corrosion process, in which the diameter is associated with the R_t . The R_t value represents the corrosion resistance [23]. At the low frequency, the second arc or tail in the Nyquist plots reveals an inductive behavior of all the samples. The diameters of capacitive arcs of the ECAP-processed ZK60 Mg alloys at the initial immersion stage are much smaller than those of the solution-treated ones, which means that the solution-treated sample has better corrosion resistance.

Figure 10 presents the R_t values by fitting the experimental Nyquist plots (in Fig. 9) using ZSimpwin commercial software (USA). The R_t value of the solution-treated ZK60 Mg alloy is much larger than that of the ECAP-processed one, i.e., the solution-treated sample keeps a higher corrosion resistance compared with the ECAP-processed sample. Furthermore, the alloy

with more ECAP passes has smaller capacitive arc and thus has poor corrosion resistance. The aged sample has a similar Nyquist plot to the ZK60 Mg alloy processed by ECAP, but its R_t value is larger than that of the ZK60 Mg alloy processed by ECAP. It should be noted that the above EIS results are in agreement with the findings from the polarization curves in Fig. 6.

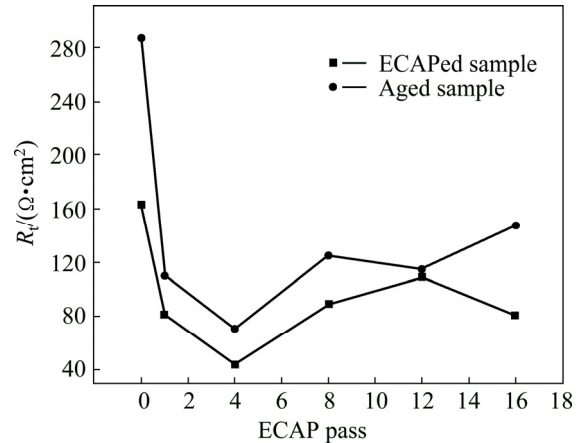


Fig. 10 R_t value of ECAP-processed samples and aged samples immersed in 3.5% NaCl solution

3.3 Scanning Kelvin probe

The potential differences between the second phases and the metallic matrix were investigated by scanning Kelvin probe force microscopy (SKPFM) [17] and the related results demonstrate that the volta potential difference between the second phases and the Mg matrix will cause the formation of galvanic couples and the occurrence of local corrosion. The SKP measures the non-contact difference in work function, according to Refs. [18–20], φ_{corr} has a simple relationship with the volta potential measured under a thin electrolyte layer.

$$\varphi_{\text{corr}} = \Delta\varphi_{\text{EL}}^{\text{Pr}} + A \quad (1)$$

where $\Delta\varphi_{\text{EL}}^{\text{Pr}}$ represents the volta potential difference between the sample surface and the probe, the constant (A) is determined by the experiment. Figure 11 shows the SKP 3D potential maps and contour maps of the solution-treated, 4p and 16p samples. Figure 12 shows the SKP potential maps and contour maps of those post-ECAP aging samples. From Figs. 11 and 12, it can be seen that the potential of all the samples essentially varies from -1.2 to -1.0 V. Since the samples before SKP tests were polished and placed in air for one night, a natural oxide film could form on the samples. The volta potential of ZK60 Mg alloy may be influenced by the presence of oxide film and thus is nobler than the corrosion potential. It is also noted that the volta potential of all the samples is distributed evenly and the active sites are distributed randomly, which demonstrates that positive and negative sites are distributed irregularly.

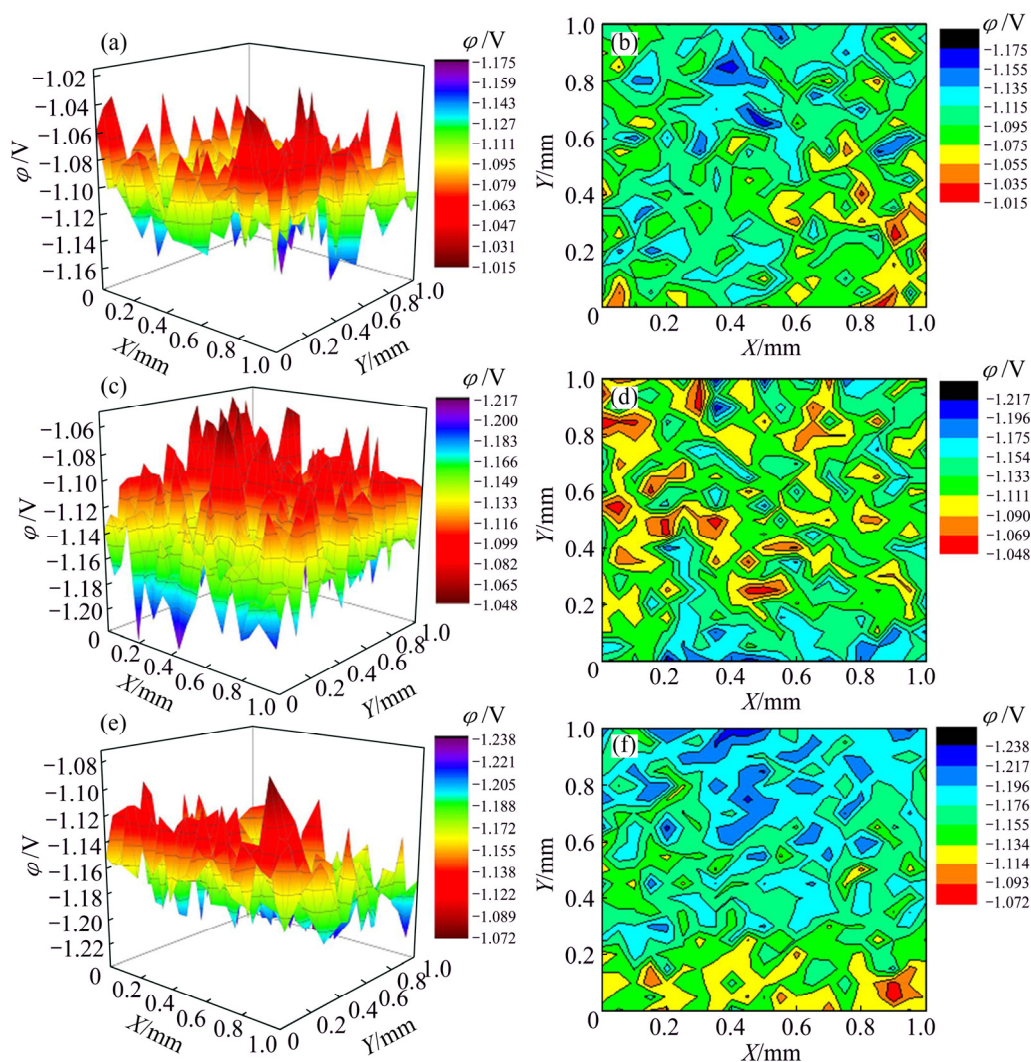


Fig. 11 SKP potential images (a, c, e) and contour maps (b, d, f) of alloy with different ECAP passes: (a, b) Solution-treated sample; (c, d) 4p sample; (e, f) 16p sample

According to Ref. [24], the data are fitted to get the degree of concentration of voltaic potential. The formula used for fitting is Gaussian equation as follows:

$$y = y_0 + \frac{B}{\sigma\sqrt{\pi/2}} \exp\left[-2\frac{(x-\mu)^2}{\sigma^2}\right] \quad (2)$$

where y_0 is the bias value of y , B is the constant of Gaussian fitting equation, μ is the center of potential, σ^2 is the concentration extent of potential. From the fitting results shown in Fig. 13, the SKP potential decreases with increasing the ECAP pass for the ECAP-processed samples and the post-ECAP aged ones; however, the potential of the post-ECAP aged sample is higher than that of the un-aged sample. Figure 14 presents that both φ_{corr} and volta potential decrease with increasing the ECAP pass. The SKP results indicate that the aged samples may have better corrosion resistance when immersed in corrosion media due to higher

electrochemical stability. The improvement of corrosion behavior after aging can be related to the redistribution of second phases and the relieving of internal stress, which changes the potential slightly and thus makes the post-ECAP aged sample form better protective film.

4 Discussion

As mentioned above, some literatures have reported that grain refinement can improve the corrosion resistance of metallic materials. The higher corrosion resistance can be related to the better protective film formed on the surface of nanocrystalline and UFG material. Unfortunately, ECAP weakens the corrosion resistance of the ZK60 Mg alloy in aqueous NaCl solution, besides the well-known strengthening and toughening effect [8,14]. This negative effect should be associated with the microstructure and corrosion mechanism of ZK60 Mg alloy processed by ECAP.

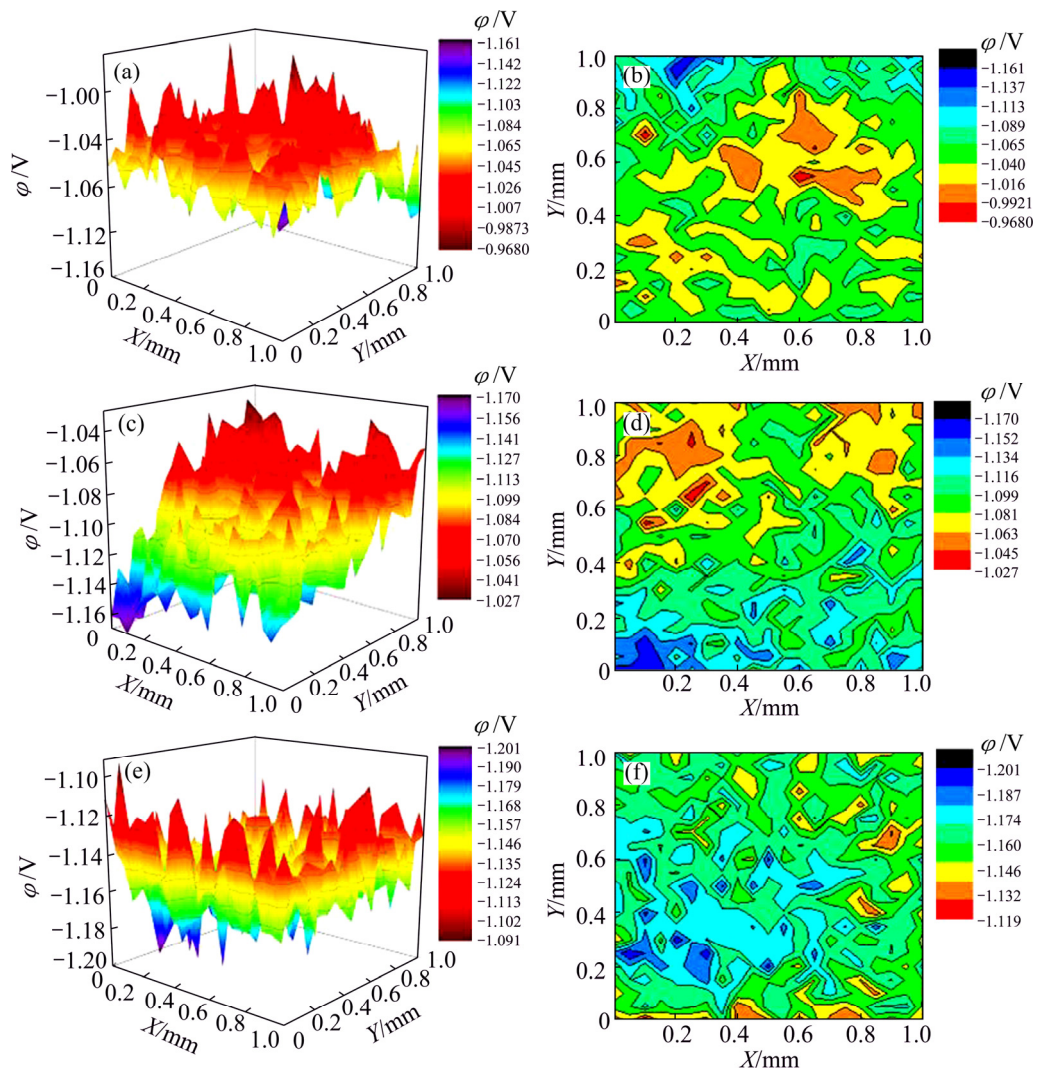


Fig. 12 SKP potential images (a, c, e) and contour maps (b, d, f) of ZK60 Mg alloy with different ECAP passes plus aging: (a, b) Solution-treated sample; (c, d) 4p sample; (e, f) 16p sample

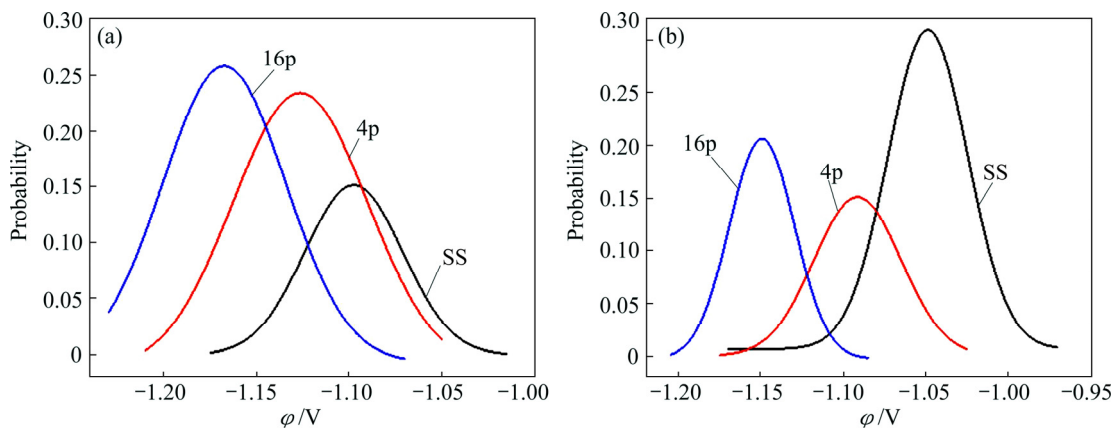


Fig. 13 Fitting lines of SKP potential of ZK60 Mg alloys with different ECAP passes (a) and after further aging (b)

The sharp decrease of the grain size provides a large fraction of grain boundaries, while more ECAP passes produces larger residual stresses and more crystalline defects and higher dislocation densities stored in the grains. Thus, the Mg alloy after multi-pass ECAP has a

higher reaction activity to the solution [9]. According to the SEM observation, the micro-crack in the corrosion products can be related to the internal stress, which was accumulated in more ECAP passes but could be reduced after aging. Thus, the internal stress of ZK60 samples

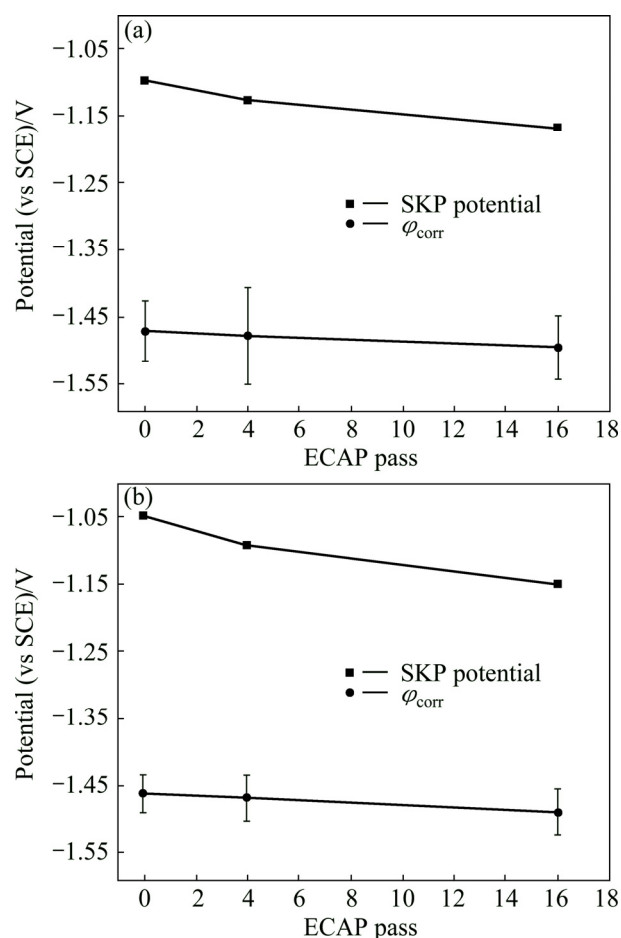


Fig. 14 Volta potential and φ_{corr} of alloy with different ECAP passes (a) and after further aging (b)

after ECAP and aging was measured by XRD (Bruker-AXS D8 Advance) on the same lattice plane {203}. The internal stress in the 4p sample after aging was calculated to be (-1.52 ± 0.23) MPa (normal stress) and the stress in the 16p sample after aging was calculated to be (-1.82 ± 0.23) MPa (normal stress). The results show that the internal stress in the samples processed by ECAP is compressive stress, and also verify that the sample with more ECAP passes does accumulate a larger compressive stress. HAMU et al [12] found that the accelerated corrosion was related with the large plastic strain imposed. LI and CHENG [25] found that the tensile stress enhanced the steel dissolution more significantly than the compressive stress. Hence, the compressive stress accumulated during ECAP passes has an effect on the corrosion resistance of ZK60 Mg alloy.

Furthermore, the corrosion behavior was also influenced by the protective ability of the corrosion-product film, which could be improved by better redistribution of the second-phase particles. According to Ref. [1], β phase is expected to act as a barrier when there is a small grain size, i.e., the low steady-state

corrosion rate approaching pure β phase can be expected from such microstructures. In contrast, the accelerated microgalvanic corrosion easily occurs when the grain size is large and the β phase is agglomerated. Figure 4 shows the SEM images of the as-cast, 4p and 16p ZK60 Mg alloy samples. It can be seen that the second-phase particles in the matrix are small and homogeneously distributed after ECAP and aging, which has a positive effect on the corrosion resistance. LI et al [26] and LIANG et al [27] have reported that aging treatment can affect the corrosion behavior by transforming the microstructure, especially the cathodic phase. LU et al [28] found that a proper aging treatment can precipitate plenty of second phases of Mg–Zn, which could inhibit the corrosion. The small second-phase particles could not act as the barriers to the corrosion but as the unstable cathode of micro-corrosion cell, which turns localized corrosion to comprehensive and uniform corrosion. The anti-corrosion improvement of ZK60 Mg alloy processed by ECAP with sequent aging also proves that the post-ECAP aging can adjust the distribution of second-phase particles, thus improving the protective capability of the corrosion-product layer and the comprehensive performances of the Mg alloy.

The oxide film and other passive films may preferably nucleate at the surface crystalline defects [29]. For ZK60 Mg alloy, the structure and stability of MgO oxide film and $\text{Mg}(\text{OH})_2$ partial-passive film have great effect on its corrosion resistance. The ZK60 Mg alloy processed by ECAP has more nucleation sites for the formation of MgO oxide film in air due to a large number of energetic crystalline defects mentioned above. Unfortunately, the oxide film on the surface of ZK60 Mg alloy processed by ECAP is still unstable in NaCl solution owing to the high internal compressive stresses, because the oxide film only has a protective ability in a certain period of time. In Fig. 5, the OCP values of all the samples immersed in the solution decrease for a certain period of time. The decrease of the OCP values is caused by the quick dissolution of the MgO oxide film in the corrosive solution. This phenomenon indicates that although ZK60 Mg alloy processed by ECAP has a higher fraction of oxide film on the surface compared with the solution-treated alloy, the overall stability becomes worse. More energetic crystalline defects in the ZK60 Mg alloy processed by ECAP provide more nucleation sites, thus making it easier to form $\text{Mg}(\text{OH})_2$ film than the solution-treated one. The 16p ZK60 Mg alloy takes the least time to reach the peak OCP value, which verifies that more ECAP passes lead to higher activity for the rapid formation of $\text{Mg}(\text{OH})_2$ film. However, $\text{Mg}(\text{OH})_2$ will react with Cl^- continuously and the corrosion product is loose and not stable, making Cl^- and water easily penetrate into the matrix.

5 Conclusions

1) Different microstructural states were obtained by solid-solution treatment, multi-pass equal-channel angular pressing and post-ECAP aging. Finer grains were achieved after ECAP and remained after aging treatment.

2) The strain-induced grain refinement with more crystalline defects deteriorates the corrosion resistance of the ZK60 Mg alloy, which can be reflected by larger J_{corr} values in the polarization curves and lower R_t values in the EIS plots. However, the corrosion behavior is improved by aging treatment. The improvement may be due to the reduction of stress and the better film protection.

3) The strain-induced crystalline defects (including subgrain boundaries) and the residual stress in the ECAP-processed alloy increase the activity of the Mg matrix, making it easier be corroded. The film formed on the UFG ZK60 Mg alloy has low protective capability due to its worse stability in a solution containing Cl^- , and the refined second-phase particles make the ZK60 Mg alloy corrosion more uniform and severer.

4) The volta potentials of all the samples distribute evenly and the active sites distribute randomly, i.e., the cathode and anode sites of the fine-grained ZK60 Mg alloy are irregular. The SKP potential decrease with increasing the ECAP pass, and the potential of the post-ECAP aged sample is higher than that of the unaged ones. It also proves that the aged samples have better corrosion resistance in comparison with the ECAP-processed ones.

References

- [1] SONG G, ATRENS A, DARGUSCH M. Influence of microstructure on the corrosion of die-cast AZ91D [J]. *Corrosion Science*, 1998, 41(2): 249–273.
- [2] ZHANG Tao, LI Ying, WANG Fu-hui. Roles of β phase in the corrosion process of AZ91D magnesium alloy [J]. *Corrosion Science*, 2006, 48(5): 1249–1264.
- [3] AMBAT R, AUNG N N, ZHOU W. Studies on the influence of chloride ion and pH on the corrosion and electrochemical behaviour of AZ91D magnesium alloy [J]. *Journal of Applied Electrochemistry*, 2000, 30(7): 865–874.
- [4] HOOG C, BIRBILIS N, ESTRIN Y. Corrosion of pure Mg as a function of grain size and processing route [J]. *Advanced Engineering Materials*, 2008, 10(6): 579–582.
- [5] ZHAO Y H, LIAO X Z, JIN Z, VALIEV R Z, ZHU Y T. Microstructures and mechanical properties of ultrafine grained 7075 Al alloy processed by ECAP and their evolutions during annealing [J]. *Acta Materialia*, 2004, 52(15): 4589–4599.
- [6] VALIEV R, LANGDON T. Principles of equal-channel angular pressing as a processing tool for grain refinement [J]. *Progress in Materials Science*, 2006, 51(7): 881–981.
- [7] CHEN Y J, WANG Q D, LIN J B, LIU M P, HJELEN J, ROVEN H J. Grain refinement of magnesium alloys processed by severe plastic deformation [J]. *Transactions of Nonferrous Metals Society of China*, 2014, 24(12): 3747–3754.
- [8] WATANABE H, MUKAI T, ISHIKAWA K, HIGASHI K. Low temperature superplasticity of a fine-grained ZK60 magnesium alloy processed by equal-channel-angular extrusion [J]. *Scripta Materialia*, 2002, 46(12): 851–856.
- [9] SONG Dan, MA Ai-bin, JIANG Jing-hua, LIN Ping-hua, YANG Dong-hui, FAN Jun-feng. Corrosion behavior of equal-channel-angular-pressed pure magnesium in NaCl aqueous solution [J]. *Corrosion Science*, 2010, 52(2): 481–490.
- [10] BALYANOV A, KUTNYAKOVA J, AMIRKHANOVA N, STOLYAROV V, VALIEV R, LIAO X Z, ZHAO Y H, JIANG Y B, XU H F, LOWE T C, ZHU Y T. Corrosion resistance of ultra fine-grained Ti [J]. *Scripta Materialia*, 2004, 51(3): 225–229.
- [11] SONG Dan, MA Ai-bin, JIANG Jing-hua, LIN Ping-hua, YANG Dong-hui. Corrosion behavior of ultra-fine grained industrial pure Al fabricated by ECAP [J]. *Transactions of Nonferrous Metals Society of China*, 2009, 19(5): 1065–1070.
- [12] HAMU G B, ELIEZER D, WAGNER L. The relation between severe plastic deformation microstructure and corrosion behavior of AZ31 magnesium alloy [J]. *Journal of Alloys and Compounds*, 2009, 468(1–2): 222–229.
- [13] MINÁRIK P, KRÁL R, JANECEK M. Effect of ECAP processing on corrosion resistance of AE21 and AE42 magnesium alloys [J]. *Applied Surface Science*, 2013, 281: 44–48.
- [14] HE Y B, PAN Q L, QIN Y J, LIU X Y, LI W B, CHIU Y L, CHEN J J. Microstructure and mechanical properties of ZK60 alloy processed by two-step equal channel angular pressing [J]. *Journal of Alloys and Compounds*, 2010, 492(1–2): 605–610.
- [15] ZHANG Yi, ZHANG Zhi-min, ZHANG Xing. Effect of aging temperature on microstructure and property of ZK60 magnesium alloys [J]. *Hot Working Technology*, 2010, 39(6): 139–142.
- [16] LI Yan, ZHANG Zhi-min, XUE Yong. Influence of aging on microstructure and mechanical properties of AZ80 and ZK60 magnesium alloys [J]. *Transactions of Nonferrous Metals Society of China*, 2011, 21(4): 739–744.
- [17] JÖNSSON M, THIERRY D, LEBOZEC N. The influence of microstructure on the corrosion behaviour of AZ91D studied by scanning Kelvin probe force microscopy and scanning Kelvin probe [J]. *Corrosion Science*, 2006, 48(5): 1193–1208.
- [18] STRATMANN M. The investigation of the corrosion properties of metals, covered with adsorbed electrolyte layers—A new experimental technique [J]. *Corrosion Science*, 1987, 27(8): 869–872.
- [19] STRATMANN M, STRECKEL H. On the atmospheric corrosion of metals which are covered with thin electrolyte layers—II. Experimental results [J]. *Corrosion Science*, 1990, 30(6–7): 697–714.
- [20] STRATMANN M, STRECKEL H, KIM K, CROCKETT S. On the atmospheric corrosion of metals which are covered with thin electrolyte layers—III. The measurement of polarisation curves on metal surfaces which are covered by thin electrolyte layers [J]. *Corrosion Science*, 1990, 30(6–7): 715–734.
- [21] PEBERE N, RIERA C, DABOSI F. Investigation of magnesium corrosion in aerated sodium sulfate solution by electrochemical impedance spectroscopy [J]. *Electrochimica Acta*, 1990, 35(2): 555–561.
- [22] CAO C N. On the impedance plane displays for irreversible electrode reactions based on the stability conditions of the steady-state—II. Two state variables besides electrode potential [J]. *Electrochimica Acta*, 1990, 35(5): 837–844.
- [23] CAO C N. On the impedance plane displays for irreversible electrode reactions based on the stability conditions of the steady-state—I. One state variable besides electrode potential [J]. *Electrochimica Acta*, 1990, 35(5): 831–836.

- [24] DONG Chao-fang, SHENG Hai, AN Ying-hui, LI Xiao-gang, XIAO Kui. Local electrochemical behavior of 2A12 aluminium alloy in the initial stage of atmospheric corrosion under Cl^- conditions [J]. Journal of University of Science and Technology Beijing, 2009, 31(7): 878–883. (in Chinese)
- [25] LI M C, CHENG Y F. Corrosion of the stressed pipe steel in carbonate–bicarbonate solution studied by scanning localized electrochemical impedance spectroscopy [J]. Electrochimica Acta, 2008, 53(6): 2831–2836.
- [26] LI Chen, PAN Qing-lin, SHI Yun-jia, WANG Ying, LI Bo. Influence of aging temperature on corrosion behavior of Al–Zn–Mg–Sc–Zr alloy [J]. Materials and Design, 2014, 55: 551–559.
- [27] LIANG Shu-quan, GUAN Di-kai, TAN Xiao-ping. The relation between heat treatment and corrosion behavior of Mg–Gd–Y–Zr alloy [J]. Materials and Design, 2011, 32(3): 1194–1199.
- [28] LU Sheng, QI Ying, WANG Ze-xin, XU Rong-yuan. Influence of aging on corrosion properties of ZK60 magnesium alloy in Cl^- alkaline solution [J]. Hot Working Technology, 2009, 38(8): 132–135.
- [29] JOHANSEN H A, ADAMS G B, RYSELBERGHE P V. Anodic oxidation of aluminum, chromium, hafnium, niobium, tantalum, titanium, vanadium, and zirconium at very low current densities [J]. Journal of the Electrochemistry Society, 1957, 104(6): 339–346.

ECAP 和时效处理对 ZK60 镁合金腐蚀行为的影响

李鑫¹, 江静华², 赵永好¹, 马爱斌², 文道静¹, 朱运田^{1,3}

1. 南京理工大学 材料科学与工程学院, 南京 210094;

2. 河海大学 力学与材料学院, 南京 210098;

3. Department of Materials Science and Engineering, NC State University, Raleigh 27695, USA

摘要: 采用多道次等通道转角挤压(ECAP)法制备 ZK60 镁合金, 并结合后续的时效处理研究晶粒细化及第二相重新分布对其腐蚀行为的影响。电化学测试结果表明: 经多道次 ECAP 后的细晶样品, 在实现强韧化的同时耐蚀性有所降低, 表现为极化曲线中较高的腐蚀电流密度(J_{corr})和电化学阻抗谱中较小的电荷转移阻抗(R_t)。扫描开尔文探针(SKPFIT)测试结果表明: 样品表面阴、阳极分布均匀, 抑制了局部腐蚀, 伏打电位差随着挤压道次的增加而下降且与腐蚀电位呈线性关系。此外, ECAP 后经时效的细晶 ZK60 镁合金样品耐蚀性有所改善, 合金综合性能的提高主要归因于应力的释放和第二相颗粒的再分布。

关键词: ZK60 镁合金; 等通道转角挤压; 时效; 耐蚀性; 细晶

(Edited by Mu-lan QIN)